Title

Bonding-Directed Crystallization of Ultra-Long One-Dimensional NbS3 van der Waals Nanowires.

Journal

Journal of the American Chemical Society, 146(33)

Authors

Lopez, Diana
Zhou, Yinong
Cordova, Dmitri
et al.

Publication Date

2024-08-21

DOI

10.1021/jacs.4c05730

Peer reviewed

JACS
JOURNAL OF THE AMERICAN CHEMICAL SOCIETY

pubs.acs.org/JACS
Communication

Bonding-Directed Crystallization of Ultra-Long One-Dimensional NbS_3 van der Waals Nanowires

Diana Lopez, Yinong Zhou, Dmitri Leo Mesoza Cordova, Griffin M. Milligan, Kaleolani S. Ogura, Ruqian Wu, and Maxx Q. Arguilla*

Cite This: J. Am. Chem. Soc. 2024, 146, 22863−22868
Read Online

ABSTRACT: The rediscovery of one-dimensional (1D) and quasi-1D (q-1D) van der Waals (vdW) crystals ushered the realization of nascent physical properties in 1D that are suitable for applications in photonics, electronics, and sensing. However, despite renewed interest in the creation and understanding of the physical properties of 1D and q-1D vdW crystals, the lack of accessible synthetic pathways for growing well-defined nanostructures that extend across several length scales remains. Using the highly anisotropic 1D vdW NbS_3−I crystal as a model phase, we present a catalyst-free and bottom-up synthetic approach to access ultralong nanowires, with lengths reaching up to 7.9 mm and with uniform thicknesses ranging from 13 to 160 nm between individual nanowires. Control over the synthetic parameters enabled the modulation of intra- and interchain growth modalities to selectively yield only 1D nanowires or quasi-2D nanoribbons. Comparative synthetic and density functional theory (DFT) studies with a closely related nondimerized phase, ZrS_3, show that the unusual preferential growth along 1D can be correlated to the strongly anisotropic bonding and dimeric nature of NbS_3−I.

Physical properties of low-dimensional materials are significantly influenced by their size, composition, and crystal structure.[1−8] Low-dimensional materials, such as graphene and transition metal dichalcogenides (TMDCs, MCh_2; M = Mo, W, Nb, Ti, etc.; Ch = S, Se, Te), have gained widespread interest owing to inherently strong covalent in-plane bonds that form confined 2D layers that are held together by weak van der Waals (vdW) forces.[1,9] Due to their anisotropic bonding nature at the monolayer limit, 2D vdW materials display unique physical properties that are often drastically altered upon exfoliation down to length scales that approach the single-atom-thick regime.[1,9−11] In lower dimensionalities, recent efforts have demonstrated the observation of nascent physical properties in one-dimensional (1D) and quasi-one-dimensional (q-1D) analogues of 2D vdW solids.[12−22] Unlike nanosheet-forming 2D materials, 1D vdW materials exfoliate into nanowires and nanoribbons, which often display anisotropic electronic and optical properties.[5−7,23]

Of these, the modular class of 1D vdW MCh_3 (M = Ti, Zr, Hf, Nb, Ta; Ch = S, Se) crystals which exhibit strong anisotropy due to covalent bonding along only one crystallographic axis has served as a reliable platform to understand the properties of subnanometer-thick 1D chains held by vdW forces.[7,23] Like TMDCs, MCh_3 crystals exhibit unique properties based on their subunit structure and packing.[3,24−28] The polymorph-rich NbS_3 phase, for example, shows electronic properties that range from semiconducting (types I, IV, VI) to metallic (types II, III, V).[24,25] It also hosts unusual properties, including near-room temperature charge density wave states with exceptional coherence,[29] field-effect responsive sliding,[30] and highly polarized optoelectronic properties.[23] The more stable NbS_3−I polymorph has a triclinic structure (P-1 space group),[31] which arises from the in-chain dimerization of Nb atoms (Figure 1A).[25] NbS_3−I is an air-stable and mechanically robust semiconducting material,[23,32,26] which displays ultrabroadband photodetection from UV (375 nm) to THz (118.8 μm), making it ideal for use in optoelectronic nanodevices.[23,32] While heavily studied in the bulk,[3,25] efforts to understand emergent properties and applications of NbS_3−I and related MCh_3 phases from quantum confinement are hampered by the stochasticity of top-down exfoliation which result in a distribution of nanowires, nanoribbons, and nanosheets (Figure S1).

Here, we sought to understand the role of anisotropic bonding and intrachain dimerization in the growth of MCh_3 crystals and investigate whether these can be leveraged to grow ultralong nanowires with high aspect ratios. We present a catalyst-free, bottom-up, and controllable vapor-phase approach to grow record-long nanowires of the MCh_3 model phase NbS_3−I, obviating the need for top-down exfoliation. Using dark-field scattering, scanning electron microscopy-energy dispersive X-ray spectroscopy (SEM-EDS), Raman spectroscopy, atomic force microscopy (AFM), and transmission electron microscopy (TEM), we confirmed the polytype and dimensions of the resulting nanowires, which reached unusually long lengths up to 7.9 mm. We rationalize this growth behavior using a DFT-guided assessment of the

Received: April 26, 2024
Revised: August 1, 2024
Accepted: August 2, 2024
Published: August 8, 2024

https://doi.org/10.1021/jacs.4c05730
J. Am. Chem. Soc. 2024, 146, 22863−22868

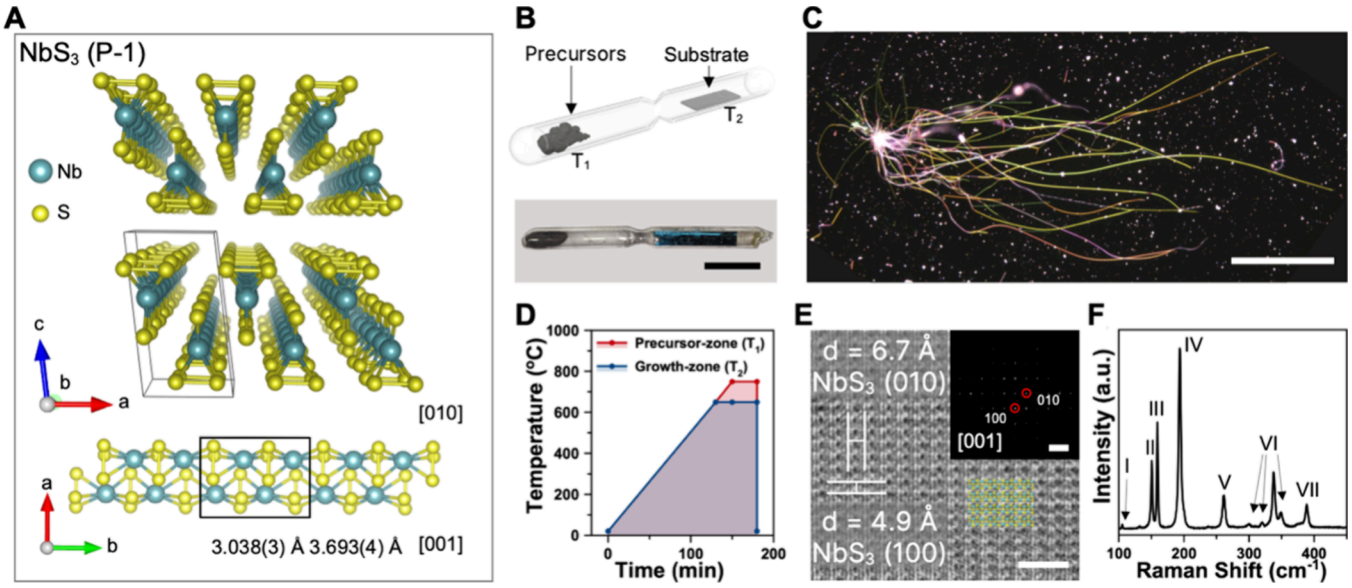

Figure 1. (A) Crystal structure of NbS_3–I and projection of parallel ([010] zone axis) and perpendicular ([001] zone axis) to the chain direction.[31] (B) Graphical representation (top) and actual ampule postreaction (bottom) used to synthesize NbS_3–I nanowires. The two regions are labeled as T_1 and T_2. Scale bar, 3 cm. (C) Dark-field optical micrograph of NbS_3–I nanowires on a Si/SiO_2 substrate. Scale bar, 245 μm. (D) Corresponding CVT furnace temperature program in the high (T_1) and low (T_2) temperature regions used to grow nanowires in C. (E) TEM image of a NbS_3–I nanowire from C with an overlaid [001]-oriented crystal model of NbS_3–I. Scale bar, 2 nm. Corresponding FFT and zone axis assignment are inset. Scale bar, 0.5 $Å^{-1}$. (F) Raman spectrum of an isolated NbS_3–I nanowire from C (532 nm excitation).

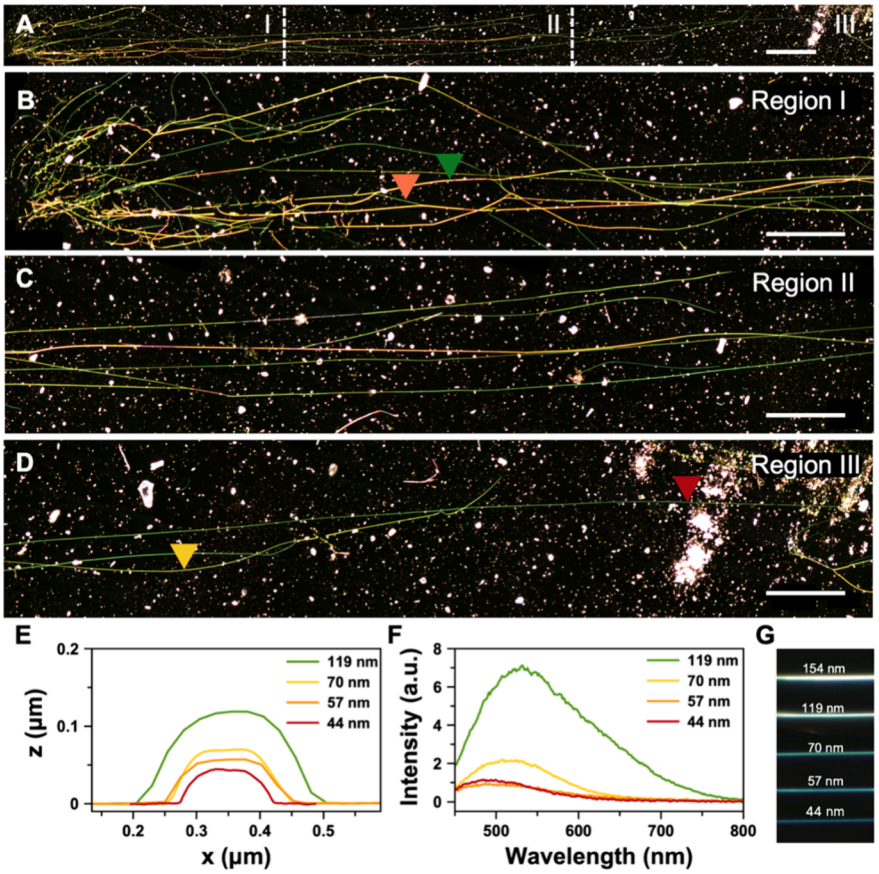

Figure 2. (A) Dark-field optical micrographs of NbS_3–I nanowires on a Si/SiO_2 substrate after a 3-day vapor-phase synthesis, divided into three regions: I, II, and III. Scale bar, 490 μm. (B, C, D) High-magnification micrographs corresponding to regions I, II, and III in A, respectively. Triangles point to the location where AFM and optical scattering spectroscopy measurements were taken; colors correspond to measurements in E and F. (E) AFM height profiles of the NbS_3–I nanowires from A. (F) Corresponding thickness-dependent dark-field optical scattering spectra of NbS_3–I nanowires in A. (G) Dark-field optical micrographs of nanowires of various thicknesses taken at 50× objective magnification.

https://doi.org/10.1021/jacs.4c05730
J. Am. Chem. Soc. 2024, 146, 22863−22868

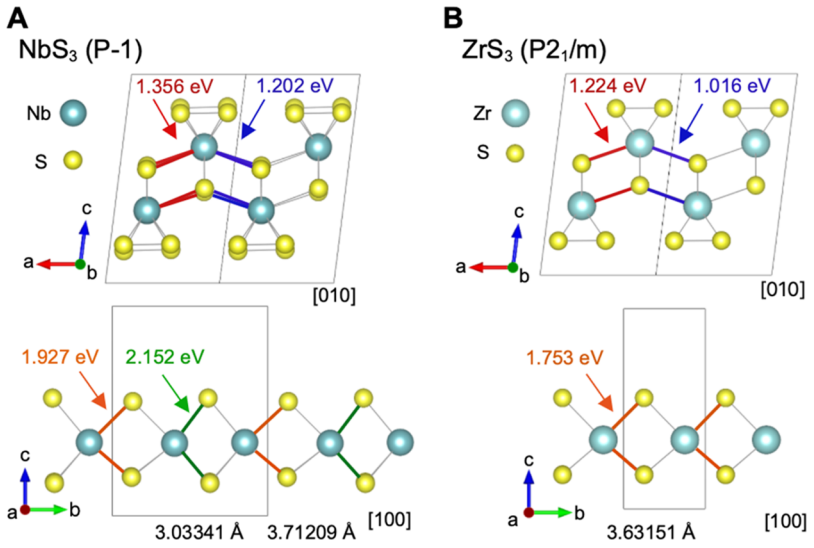

Figure 3. (A, top) DFT-calculated interchain bonding energies of NbS_3−I within (red) and across (blue) the unit cell along the *a* axis. (A, bottom) DFT-calculated bonding energies of the covalent intrachain interactions in NbS_3−I. There are two bonding energies (orange and green bonds) corresponding to the nonequivalent intrachain interactions arising from Nb−Nb dimerization along the *b* axis. (B, top) DFT-calculated interchain bonding energies of ZrS_3 within (red) and across (blue) the unit cell along the *a* axis. (B, bottom) DFT-calculated bonding energies corresponding to the covalent intrachain interactions in ZrS_3 (orange).

anisotropic intra- and interchain bonding, which highlights the pronounced role of phase stability and intrachain dimerization in distinctly promoting in-chain growth.

NbS_3−I nanowires were grown using a modified chemical vapor transport (CVT) method previously reported by Hu et al. for 2D vdW crystals, where the reaction ampule was narrowed near the center to grow thin nanoscale structures on a suitable substrate.[33] Here, we significantly modified several parameters, including reaction ampule dimensions, the substrate, and the temperature profile, to precisely grow NbS_3−I nanostructures (Figure 1B,D). For all syntheses, elemental Nb and S powder loadings followed an optimized Nb/S ratio of 1:4, as we found that excess sulfur acts as a transport agent and suppresses the growth of the competing 2D phase, NbS_2 (Figures S2, S3). Necking the center of the ampule tuned the precursor flux to the substrate (Figure S4). Reports on the CVT synthesis of bulk NbS_3−I were able to use close-to-stoichiometric ratios because of longer reaction times of 5 days to 2 weeks,[3,23,24,32,34] which facilitate complete reaction and precursor mixing. However, when growing nanostructures on shorter reaction time scales (30 min to 3 days), higher sulfur partial pressures are necessary to grow the target sulfur-rich NbS_3. Bulk, needle-like crystals with smooth facets formed on the inner top surface of the quartz ampule, whereas the targeted nanowires were deposited on the Si/SiO_2 substrate (Figures S5−S7). Generally, we observed that thin nanowires grew radially from localized nucleation spots and along the substrate edges, resulting in comparable cross-sections across the substrate (Figure 1C; Figure S7, Table S1).

TEM, EDS, and Raman spectroscopy demonstrated that bulk crystals and nanowires belong to the NbS_3−I polytype (Figure 1E,F; Figures S6, S8). For all nanowires in Figure 1C, EDS analysis confirmed the composition of single, isolated nanowires composed of Nb and S elements with an Nb/S average ratio of ∼1:3 (Table S1). EDS mapping showed uniform distribution of Nb and S across the nanowires (Figure S8). Dark-field optical images of the substrate showed nanowires with high aspect ratios emerging from few nucleation spots (Figure 1C). TEM imaging shows the high crystallinity of the nanowires with *d*-spacing matching that of NbS_3−I and their flexibility (Figure 1E; Figures S6, S9). The fast Fourier transform (FFT) was indexed as the NbS_3−I [001] zone axis (Figure 1E). Peaks in the Raman spectrum of the nanowires in Figure 1C (Figure 1F) are consistent with the NbS_3−I polytype.[28,35] X-ray photoelectron spectroscopy (XPS) of bulk crystals showed peaks corresponding to the $3d_{3/2}$ and $3d_{5/2}$ states of Nb and the S′ $2p_{1/2}$, S′ $2p_{3/2}$ and the S $2p_{1/2}$, S $2p_{3/2}$ states of S (Figure S10). Assignments of Raman peaks I to VII are in the Supporting Information.

We systematically varied the duration of the reactions from 30 min to 3 days at a fixed temperature gradient (T_1 = 750 °C to T_2 = 650 °C) to further understand the effect of time on the growth of NbS_3−I. Generally, the growth of NbS_3−I nanowires was observed at all reaction times used in this study. If the reaction is quenched using an ice bath, the nanowires would be shorter than the naturally cooled analogues. Nanowires from a quenched 30 min reaction reached lengths of up to ∼1 mm, with most nanowires having lengths between 30 and 249 μm and heights ranging from 13 nm to ∼100 nm (Figure 1C). In contrast, a 30 min reaction with natural cooling yielded nanowires with lengths up to ∼2.5 mm, with most lengths between 69 and 728 μm and with comparable heights from 24 nm to ∼100 nm (Figure S7, S17). Intriguingly, a three-day reaction time with natural cooling yielded ultralong nanowires of up to ∼7.9 mm in length, with most lengths ranging from 251 μm to 2.2 mm and heights of 40 to 160 nm (Figure 2A−E, S17). Our ability to grow well-defined NbS_3−I nanowires enabled us to measure their thickness-dependent optical scattering properties (Figure 2F,G). From dark-field hyperspectral imaging and spectroscopy, we found thickness-dependent spectral features in nanowires that are ∼40- to 120-nm-thick, illustrating that the frequency distribution of scattered light can be systematically modulated by controlling the nanowire thickness (Figure 2F). Generally, nanowires that were sub-100-nm-thick appeared green-blue, whereas thicker

https://doi.org/10.1021/jacs.4c05730
J. Am. Chem. Soc. 2024, 146, 22863−22868

nanowires (>100 nm) appeared yellow-white in the dark-field micrographs (Figure 2G).

We found that the morphology of the NbS_3−I nanostructures could also be modulated by adjusting the temperature and duration of the synthetic steps to promote a sulfur-rich environment (Figures S11, S12; Supplementary Text). We observed that this program promoted lateral growth of the chains along the *a* axis (vdW direction), which uniquely yielded wide nanoribbon analogues of NbS_3−I (Figures S13, S14). Peaks in the Raman spectra of the nanoribbons, like the nanowires, agreed well with NbS_3−I phonon modes (Figure S15). Nanoribbons crystallized into long and thin structures with dimensions ranging from 88 nm × 10 μm × 640 μm to 91 nm × 37 μm × 1200 μm (Figures S13, S14, S16, and S17). Nanoribbons display shorter lengths compared to nanowires (Figure S17). EDS analysis confirmed a Nb/S ratio of ∼1:3, and like the nanowires, mapping showed an even distribution of Nb and S throughout the crystal (Figure S18). The distinction between nanowire and nanoribbon growths is discussed in the Supplementary Text.

To understand the unusual growth behavior of NbS_3−I, we directly applied methods used to grow NbS_3−I to a closely related MCh_3 phase, ZrS_3. ZrS_3 displays the same trigonal prismatic coordination environment along the chain and strong covalent bonding along the *b* axis, but without the in-chain metal−metal dimerization (Figure S19). Crystals found on the substrate were nanoribbons significantly shorter than NbS_3−I. The nanoribbons had thicknesses ranging from ∼6 to 200 nm and lengths ranging from 0.056 to 1.8 μm, which are at least 3 orders of magnitude shorter than NbS_3−I nanowires (Figure S20). Raman spectroscopy (Figure S21) and TEM (Figure S22) confirmed that the crystal structure of the nanocrystals is consistent with that of ZrS_3.

We performed density functional theory (DFT) calculations to analytically compare bond strengths of NbS_3−I and ZrS_3 across multiple crystallographic directions and rationalize the disparity between the growth of ultralong NbS_3−I nanowires versus the significantly shorter ZrS_3 nanoribbons (Figure 3; Figures S23−S30; Table S2). Partial filling of the d-orbital bands in NbS_3 (d^1), as opposed to ZrS_3 (d^0), leads to in-chain Nb−Nb interactions, which split the band and decrease the overall energy (Figures S29, S30).[36] This is evidenced by the overall stronger bonding in NbS_3−I (Figure 3). For NbS_3−I, calculated intrachain bonding strengths of 1.927 eV (orange; Figure 3A) and 2.152 eV (green; Figure 3A) were significantly higher than the calculated intrachain bonding strength of 1.753 eV in ZrS_3 (orange; Figure 3B). Enhancement of the intrachain bonding strength reaches 0.4 eV and is significantly higher than the enhancement along other directions (<0.2 eV; Table S2). This increase in covalent intrachain bonding strength is primarily attributable to in-chain dimerization of Nb atoms. Calculations were also performed to understand the origin of the dimerization and stability of NbS_3−I. We constructed the NbS_3−V polytype,[3,25] a metastable $P2_1/m$ polymorph with a nondimerized structure like ZrS_3 (Figure S29B). The additional electron in Nb, compared to Zr, introduces two extra electrons per unit cell. This lifts the Fermi level, leading to a metallic state in NbS_3−V (Figure S29D,E). Comparing NbS_3−I to NbS_3−V, we found that (1) dimerization in NbS_3−I lowers the total energy (E) of the system by 0.18 eV, calculated as $2E(NbS_3\text{-V}) - E(NbS_3\text{-I})$, and (2) dimerization, reminiscent of Peierls-induced transition,[25] opens an indirect band gap in NbS_3−I (Figure S29F).[26,27] We posit that the stable in-chain dimerization likely influences the preferential bottom-up growth of NbS_3−I nanocrystals along the chain direction.

■ ASSOCIATED CONTENT

Supporting Information

The Supporting Information is available free of charge at https://pubs.acs.org/doi/10.1021/jacs.4c05730.

Supplementary text; materials and methods; and additional sample micrographs, spectroscopic results, reaction schematics, and computational band structures and densities of states (PDF)

■ AUTHOR INFORMATION

Corresponding Author

Maxx Q. Arguilla − *Department of Chemistry, University of California Irvine, Irvine, California 92697, United States;* orcid.org/0000-0001-9948-0814; Email: marguill@uci.edu

Authors

Diana Lopez − *Department of Chemistry, University of California Irvine, Irvine, California 92697, United States*

Yinong Zhou − *Department of Physics and Astronomy, University of California Irvine, Irvine, California 92697, United States*

Dmitri Leo Mesoza Cordova − *Department of Chemistry, University of California Irvine, Irvine, California 92697, United States;* orcid.org/0000-0002-7527-8950

Griffin M. Milligan − *Department of Chemistry, University of California Irvine, Irvine, California 92697, United States;* orcid.org/0000-0002-6632-8004

Kaleolani S. Ogura − *Department of Chemistry, University of California Irvine, Irvine, California 92697, United States*

Ruqian Wu − *Department of Physics and Astronomy, University of California Irvine, Irvine, California 92697, United States;* orcid.org/0000-0002-6156-7874

Complete contact information is available at: https://pubs.acs.org/10.1021/jacs.4c05730

Author Contributions

All authors have given approval to the final version of the manuscript.

Notes

The authors declare no competing financial interest.

■ ACKNOWLEDGMENTS

This work was supported by the National Science Foundation under award No. DMR-2340918. D.L. and G.M.M. are funded by the National Science Foundation through the NSF Graduate Research Fellowship Program, fellow ID: 2023354005 and 2023331840, respectively. Y.Z. and R.W. are supported by the National Science Foundation Materials Research Science and Engineering Center program through the UC Irvine Center for Complex and Active Materials under the award number DMR-2011967 and the Department of Energy, Office of Basic Energy Sciences, under award number DE-FG02-05ER46237. Computer simulations were performed at NERSC. The authors acknowledge the UC Irvine Department of Chemistry Laser Spectroscopy Laboratories and its director, Prof. Dmitry Fishman, for instrument support. Several aspects of this work were performed at the UC Irvine Materials Research Institute (IMRI). Facilities and instrumen-

tation at IMRI are supported, in part, by the National Science Foundation through the UC Irvine Materials Research Science and Engineering Center grant number DMR-2011967. XPS work was performed using instruments funded, in part, by the National Science Foundation Major Research Instrumentation Program grant number CHE-1338173.

REFERENCES

(1) Zhao, B.; Shen, D.; Zhang, Z.; Lu, P.; Hossain, M.; Li, J.; Li, B.; Duan, X. 2D Metallic Transition-Metal Dichalcogenides: Structures, Synthesis, Properties, and Applications. *Adv. Funct. Mater.* **2021**, *31*, 2105132.

(2) Balandin, A. A.; Kargar, F.; Salguero, T. T.; Lake, R. K. One-Dimensional van Der Waals Quantum Materials. *Mater. Today.* **2022**, *55*, 74−91.

(3) Bloodgood, M. A.; Wei, P.; Aytan, E.; Bozhilov, K. N.; Balandin, A. A.; Salguero, T. T. Monoclinic Structures of Niobium Trisulfide. *APL Mater.* **2018**, *6* (2), 026602.

(4) Law, M.; Goldberger, J.; Yang, P. Semiconductor Nanowires and Nanotubes. *Annu. Rev. Mater. Res.* **2004**, *34*, 83−122.

(5) Hayden, O.; Agarwal, R.; Lieber, C. M. Nanoscale Avalanche Photodiodes for Highly Sensitive and Spatially Resolved Photon Detection. *Nat. Mater.* **2006**, *5* (5), 352−356.

(6) Huang, Y.; Duan, X.; Lieber, C. M. Nanowires for Integrated Multicolor Nanophotonics. *Small.* **2005**, *1* (1), 142−147.

(7) Island, J. O.; Molina-Mendoza, A. J.; Barawi, M.; Biele, R.; Flores, E.; Clamagirand, J. M.; Ares, J. R.; Sánchez, C.; van der Zant, H. S. J.; D'Agosta, R.; Ferrer, I. J.; Castellanos-Gomez, A. Electronics and Optoelectronics of Quasi-1D Layered Transition Metal Trichalcogenides. *2D Mater.* **2017**, *4* (2), 022003.

(8) Hannon, J. B.; Kodambaka, S.; Ross, F. M.; Tromp, R. M. The Influence of the Surface Migration of Gold on the Growth of Silicon Nanowires. *Nature.* **2006**, *440* (7080), 69−71.

(9) Mas-Ballesté, R.; Gómez-Navarro, C.; Gómez-Herrero, J.; Zamora, F. 2D Materials: To Graphene and Beyond. *Nanoscale.* **2011**, *3* (1), 20−30.

(10) Yang, R.; Fan, Y.; Zhang, Y.; Mei, L.; Zhu, R.; Qin, J.; Hu, J.; Chen, Z.; Hau Ng, Y.; Voiry, D.; Li, S.; Lu, Q.; Wang, Q.; Yu, J. C.; Zeng, Z. 2D Transition Metal Dichalcogenides for Photocatalysis. *Angew. Chem., Int. Ed.* **2023**, *135*, e202218016.

(11) Hernandez Ruiz, K.; Wang, Z.; Ciprian, M.; Zhu, M.; Tu, R.; Zhang, L.; Luo, W.; Fan, Y.; Jiang, W. Chemical Vapor Deposition Mediated Phase Engineering for 2D Transition Metal Dichalcogenides: Strategies and Applications. *Small Science.* **2022**, *2*, 2100047.

(12) Pfister, D.; Schäfer, K.; Ott, C.; Gerke, B.; Pöttgen, R.; Janka, O.; Baumgartner, M.; Efimova, A.; Hohmann, A.; Schmidt, P.; Venkatachalam, S.; van Wüllen, L.; Schürmann, U.; Kienle, L.; Duppel, V.; Parzinger, E.; Miller, B.; Becker, J.; Holleitner, A.; Weihrich, R.; Nilges, T. Inorganic Double Helices in Semiconducting SnIP. *Adv. Mater.* **2016**, *28* (44), 9783−9791.

(13) Farley, K. E.; Shi, Z.; Sambandamurthy, G.; Banerjee, S. Charge Density Waves in Individual Nanoribbons of Orthorhombic-TaS_3. *Phys. Chem. Chem. Phys.* **2015**, *17* (28), 18374−18379.

(14) Qu, Y.; Arguilla, M. Q.; Zhang, Q.; He, X.; Dincă, M. Ultrathin, High-Aspect Ratio, and Free-Standing Magnetic Nanowires by Exfoliation of Ferromagnetic Quasi-One-Dimensional van Der Waals Lattices. *J. Am. Chem. Soc.* **2021**, *143* (46), 19551−19558.

(15) Fu, B.; Wang, H. W.; Shen, S. Q. Dirac Polarons and Resistivity Anomaly in $ZrTe_5$ and $HfTe_5$. *Phys. Rev. Lett.* **2020**, *125* (25), 256601.

(16) Lu, Y. F.; Kono, H.; Larkin, T. I.; Rost, A. W.; Takayama, T.; Boris, A. V.; Keimer, B.; Takagi, H. Zero-Gap Semiconductor to Excitonic Insulator Transition in Ta_2NiSe_5. *Nat. Commun.* **2017**, *8*, 14408.

(17) Lin, C.; Ochi, M.; Noguchi, R.; Kuroda, K.; Sakoda, M.; Nomura, A.; Tsubota, M.; Zhang, P.; Bareille, C.; Kurokawa, K.; Arai, Y.; Kawaguchi, K.; Tanaka, H.; Yaji, K.; Harasawa, A.; Hashimoto, M.; Lu, D.; Shin, S.; Arita, R.; Tanda, S.; Kondo, T. Visualization of the Strain-Induced Topological Phase Transition in a Quasi-One-Dimensional Superconductor $TaSe_3$. *Nat. Mater.* **2021**, *20* (8), 1093−1099.

(18) Yue, B.; Zhong, W.; Deng, W.; Wen, T.; Wang, Y.; Yin, Y.; Shan, P.; Wang, J. T.; Yu, X.; Hong, F. Insulator-to-Superconductor Transition in Quasi-One-Dimensional HfS_3 under Pressure. *J. Am. Chem. Soc.* **2023**, *145* (2), 1301−1309.

(19) Kargar, F.; Barani, Z.; Sesing, N. R.; Mai, T. T.; Debnath, T.; Zhang, H.; Liu, Y.; Zhu, Y.; Ghosh, S.; Biacchi, A. J.; Da Jornada, F. H.; Bartels, L.; Adel, T.; Hight Walker, A. R.; Davydov, A. V.; Salguero, T. T.; Lake, R. K.; Balandin, A. A. Elemental Excitations in MoI3 One-Dimensional van Der Waals Nanowires. *Appl. Phys. Lett.* **2022**, *121* (22), 221901.

(20) Liu, G.; Rumyantsev, S.; Bloodgood, M. A.; Salguero, T. T.; Shur, M.; Balandin, A. A. Low-Frequency Electronic Noise in Quasi-1D $TaSe_3$ van Der Waals Nanowires. *Nano Lett.* **2017**, *17* (1), 377−383.

(21) Cordova, D. L. M.; Chua, K.; Huynh, R. M.; Aoki, T.; Arguilla, M. Q. Anisotropy-Driven Crystallization of Dimensionally Resolved Quasi-1D Van Der Waals Nanostructures. *J. Am. Chem. Soc.* **2023**, *145* (41), 22413−22424.

(22) Cordova, D. L. M.; Zhou, Y.; Milligan, G. M.; Cheng, L.; Kerr, T.; Ziller, J.; Wu, R.; Arguilla, M. Q. Sensitive Thermochromic Behavior of InSeI, a Highly Anisotropic and Tubular 1D van Der Waals Crystal. *Adv. Mater.* **2024**, *36*, 2312597.

(23) Wang, Y.; Wu, P.; Wang, Z.; Luo, M.; Zhong, F.; Ge, X.; Zhang, K.; Peng, M.; Ye, Y.; Li, Q.; Ge, H.; Ye, J.; He, T.; Chen, Y.; Xu, T.; Yu, C.; Wang, Y.; Hu, Z.; Zhou, X.; Shan, C.; Long, M.; Wang, P.; Zhou, P.; Hu, W. Air-Stable Low-Symmetry Narrow-Bandgap 2D Sulfide Niobium for Polarization Photodetection. *Adv. Mater.* **2020**, *32* (45), 2005037.

(24) Bloodgood, M. A.; Ghafouri, Y.; Wei, P.; Salguero, T. T. Impact of the Chemical Vapor Transport Agent on Polymorphism in the Quasi-1D NbS_3 system. *Appl. Phys. Lett.* **2022**, *120* (17), 173103.

(25) Conejeros, S.; Guster, B.; Alemany, P.; Pouget, J. P.; Canadell, E. Rich Polymorphism of Layered NbS_3. *Chem. Mater.* **2021**, *33*, 5449−5463.

(26) Dusabe, B.; Dongho-Nguimdo, G. M.; Joubert, D. P. Pressure Effect on Structural Stability and Optical Absorption of Triclinic NbS_3 from DFT and Many-Body Perturbation Calculations. *Eur. Phys. J. B* **2020**, *93* (7), 1−12.

(27) Artemkina, S. B.; Grayfer, E. D.; Kozlova, M. N.; Kozlova, S. G.; Ryzhikov, M. R.; Shein, I. R.; Fedorov, V. E. Metal-Metal Bond Excitation in Colloidal Solution of NbS_3. *Spectrochim. Acta. A Mol. Biomol. Spectrosc.* **2017**, *179*, 46−50.

(28) Fedorov, V. E.; Artemkina, S. B.; Grayfer, E. D.; Naumov, N. G.; Mironov, Y. V.; Bulavchenko, A. I.; Zaikovskii, V. I.; Antonova, I. V.; Komonov, A. I.; Medvedev, M. V. Colloidal Solutions of Niobium Trisulfide and Niobium Triselenide. *J. Mater. Chem. C Mater.* **2014**, *2* (28), 5479−5486.

(29) Zybtsev, S. G.; Pokrovskii, V. Ya.; Nasretdinova, V. F.; Zaitsev-Zotov, S. V.; Pavlovskiy, V. V.; Odobesco, A. B.; Pai, W. W.; Chu, M.-W.; Lin, Y. G.; Zupanič, E.; van Midden, H. J. P.; Šturm, S.; Tchernychova, E.; Prodan, A.; Bennett, J. C.; Mukhamedshin, I. R.; Chernysheva, O. V.; Menushenkov, A. P.; Loginov, V. B.; Loginov, B. A.; Titov, A. N.; Abdel-Hafiez, M. NbS_3: A Unique Quasi-One-Dimensional Conductor with Three Charge Density Wave Transitions. *Phys. Rev. B* **2017**, *95* (3), 035110.

(30) Taheri, M.; Sesing, N.; Salguero, T. T.; Balandin, A. A. Electric-Field Modulation of the Charge-Density-Wave Quantum Condensate in h- BN/NbS_3 Quasi-2D/1D Heterostructure Devices. *Appl. Phys. Lett.* **2023**, *123* (23), 233101.

(31) Rijnsdorp, J.; Jellinek, F. The Crystal Structure of Niobium Trisulfide, NbS_3. *J. Solid State Chem.* **1978**, *25* (4), 325−328.

(32) Wu, W.; Wang, Y.; Niu, Y.; Wang, P.; Chen, M.; Sun, J.; Wang, N.; Wu, D.; Zhao, Z. Thermal Localization Enhanced Fast Photothermoelectric Response in a Quasi-One-Dimensional Flexible NbS_3 Photodetector. *ACS Appl. Mater. Interfaces* **2020**, *12* (12), 14165−14173.

https://doi.org/10.1021/jacs.4c05730
J. Am. Chem. Soc. 2024, 146, 22863−22868

(33) Hu, D.; Xu, G.; Xing, L.; Yan, X.; Wang, J.; Zheng, J.; Lu, Z.; Wang, P.; Pan, X.; Jiao, L. Two-Dimensional Semiconductors Grown by Chemical Vapor Transport. *Angew. Chem., Int. Ed.* **2017**, *56* (13), 3611−3615.
(34) Pokrovskii, V. Y.; Zybtsev, S. G.; Nikitin, M. V.; Gorlova, I. G.; Nasretdinova, V. F.; Zaitsev-Zotov, S. V. High-Frequency, "quantum" and Electromechanical Effects in Quasi-One-Dimensional Charge Density Wave Conductors. *Physics-Uspekhi* **2013**, *56* (1), 3611−3615.
(35) Sourisseau, C.; Cavagnat, R.; Fouassier, M.; Maraval, P. Electronic, Vibrational and Resonance Raman Spectra of the Layered Semiconducting Compound NbS_3. *J. Raman Spectrosc.* **1990**, *21* (6), 337−349.
(36) Jellinek, F. Transition Metal Chalcogenides. Relationship between Chemical Composition, Crystal Structure and Physical Properties. *Reactivity of Solids* **1988**, *5* (4), 323−339.

https://doi.org/10.1021/jacs.4c05730
J. Am. Chem. Soc. 2024, 146, 22863−22868